Powder Technology 275 (2015) 131–138

Contents lists available at ScienceDirect

Powder Technology

journal homepage: www.elsevier.com/locate/powtec

A discrete-continuous approach to describe $CaCO_3$ decarbonation in non-steady thermal conditions

Edoardo Copertaro [a,*], Paolo Chiariotti [a], Alvaro A. Estupinan Donoso [b], Nicola Paone [a], Bernhard Peters [b], Gian Marco Revel [a]

[a] Universitá Politecnica delle Marche, Faculty of Engineering, Via Breccie Bianche 12, 60131 Ancona, Italy
[b] Université du Luxembourg, Faculté des Sciences, de la Technologie et de la Communication, Campus Kirchberg, 6 rue Coudenhove-Kalergi, L-1359 Luxembourg, Luxembourg

ARTICLE INFO

Article history:
Received 27 October 2014
Received in revised form 28 January 2015
Accepted 31 January 2015
Available online 10 February 2015

Keywords:
Computational Fluid Dynamics
CFD
Extended Discrete Element Method
XDEM
Discrete Particle Method
Soft sensors

ABSTRACT

In cement production, direct measurements of thermal and chemical variables are often unfeasible as a consequence of aggressive environments, moving parts and physical inaccessibility, and therefore prediction models are essential tools in these types of industrial applications. This article addresses the problem of the numerical prediction of the $CaCO_3$ calcination process, which is the first and the most energy expensive process in clinker production.
This study was conducted using the Extended Discrete Element Method (XDEM), a framework which allows a Eulerian approach for the gas phase to be combined with a Lagrange one for the powder phase.
A detailed validation of the numerical model was performed by comparison to non-isothermal TG curves for mass loss during the $CaCO_3$ decarbonation process. The complex three-dimensional predictions for solid and gas phases are believed to represent a first step towards a new insight into the cement production process.
Thus, the high accuracy and detailed description of the problem addressed, serve as a basis to assess the uncertainty of more simplified models such as those used in soft sensors.

1. Introduction

Calcium carbonate ($CaCO_3$) is a chemical compound commonly found in nature. Calcite is its most common crystalline form, and can be found in nature as the major constituent of limestone, a sedimentary rock.

Among all the applications that its production is addressed to, the most important is the cement industry; on its own this sector represents about 25% of the global demand. The Portland Cement Association expects cement consumption to reach nearly 86 Mt in 2014 [1].

Portland cement, which is the most common type of cement, is obtained by grinding a mixture of gypsum and clinker. The latter is produced by a pyroprocessing treatment, performed in precalciner kilns, and consists of heating up to a sintering temperature of about 1500°C a pre-grinded raw mix, of which limestone constitutes the major component.

Several chemical reactions occur during the heating of this material. The first is calcination, which starts around 840 °C and is almost completed inside the calciner:

$$CaCO_3 \rightarrow CaO + CO_2 \quad \Delta H = 178\ \frac{kJ}{mol}. \tag{1}$$

Calcination is a high endothermic reaction and, as a consequence, it requires a remarkable quantity of energy in order to be completed. For that reason up to 70% or more of the total fuel used for clinker production is burned in the calciner. Moreover, calcination has a strong impact on plant emissions because it represents the main source of CO_2 together with fuel burning.

The clinker production process is very complex. Currently, there is no complete description of all the factors involved in this process, owing to the complex thermal and chemical phenomena which take place. The lack of direct measurements on many process variables, as a result of several technical difficulties (e.g. moving parts, aggressive environment) also has a role in making this process difficult to understand. These factors have contributed to this process being considered as a black box, where success is entrusted to the experience of the operator and to fuzzy control strategies [2]. There is great interest in optimizing the clinker production process, because of its high-energy demand, its low efficiency and the high emissions it is characterized by. A constant

* Corresponding author. Tel.: +39 3386581667.
E-mail addresses: e.copertaro@univpm.it (E. Copertaro), p.chiariotti@univpm.it (P. Chiariotti), alvaro@estupinan.net (A.A. Estupinan Donoso), n.paone@univpm.it (N. Paone), bernhard.peters@uni.lu (B. Peters), gm.revel@univpm.it (G.M. Revel).

http://dx.doi.org/10.1016/j.powtec.2015.01.072
0032-5910/

price increase for fossil fuels, as well as increasingly severe environmental regulations, is therefore inducing world cement producers to optimize their processes and to verify that they are continuously run in optimized conditions [3].

Within this context the development of advanced and accurate numerical models, able to predict all the complex thermal and chemical phenomena involved, is gaining relevance. The complexity of these models is also increased by materials that are in different states, i.e. gaseous, liquid and solid, as well as powder. Besides providing predictions, these models could also furnish theoretical support for new measurement strategies based on soft-sensors. Soft sensors — also known as software sensors or neural-network-inferential calculators — are mathematical models, which provide a correlation of non-measured variables with others that are measured. In the last two decades soft sensors have become recognized as a valid alternative to traditional methods for the acquisition of critical process variables [4]. They appear particularly suited for processes like cement production, where difficulties in the measurement of particular variables (temperature profile of the material inside the kiln, evolution of the chemical species inside the kiln, etc.) are counterbalanced by a relevant number of measurements on other variables (temperature on the external shell, temperature at the inlet and the outlet, chemical composition at the inlet and the outlet, etc.).

$CaCO_3$ calcining has been extensively studied [5]. According to the results obtained by different authors the apparent magnitude of the Arrhenius parameters range from 110 to 3800 kJ/mol for the activation energy, and from 10^2 to 10^{157} S^{-1} for the frequency factor. Gieorgieva [5] concludes that wide variations in the values can be ascribed to the shape of the crystalline phase, the mean size of the particles, the sample mass, isothermal or non-isothermal heating, the heating rate, the static or dynamic atmosphere around the sample, the furnace atmosphere, the partial pressure of carbon dioxide, and the particular calculation procedure adopted.

Mikulcic [6] presented a numerical modeling of the calcination reaction mechanism for cement production using a CFD code to simulate turbulent flow, temperature, concentration fields of the reactants and products, as well as the interaction of particles with the gas phase. In his review he found that the first mathematical model for calcination mechanisms was developed by Borgwart [7], who concluded that the reaction rate is determined by heat and mass transfer inside a particle. Bes [8] proposed a 3-stage model for $CaCO_3$ calcination in cement calciners. A study by Mohr [9] describes the mathematical model of the calcination process, showing the impact of various parameters in the rate of calcination. Several CFD models have been developed, in order to describe heat and mass transport inside cyclone heat exchangers. According to Slack [10], almost all CFD models for cyclone heat exchangers are based on the Reynolds Stress Turbulence Model or Large Eddy Simulation. Hillers investigated the influence of several turbulence models on the calcination results using the same calcination model. Hu [11] provided a combined Eulerian Lagrangian approach for numerical modeling of a cement calciner, where the gas phase was modeled according to a $k-\epsilon$ model, particle dynamics were accounted for by a stochastic trajectories model, and a shrink core model surface controlling reaction was used for raw meal calcination.

This paper presents an Extended Discrete Element Method (XDEM) approach to predict $CaCO_3$ decomposition.

The Extended Discrete Element Method has successfully been used to study different thermochemical processes that appear during industrial processes. Estupinan [12] successfully applied XDEM in the prediction of heterogeneous reactions in packed beds. Estupinan et al. [13] applied XDEM techniques to model heat transfer in packed beds. XDEM simulations for water removal in packed beds were reported by Peters [14] and Mahmoudi et al. [15]. Peters [16–18] predicted the complex thermochemical processes of pyrolysis by the XDEM concept. Hoffman et al. [19,20] reviewed iron oxide reduction by using the same XDEM approach. Similarly, a CFD–DEM numerical investigation on heat and mass transfer related to the chemical conversion of limestone into quicklime in shaft kilns was proposed by Bluhm-Drenhaus [21]. However, in the latter, conductive and radiative heat transfer between the particles and the walls was not taken into account. This certainly affects heat transfer and may be worthwhile for certain cases. Nevertheless, Bluhm-Drenhaus [21] presents a setup that provides results in good agreement with experimental data.

Consequently, this paper describes the application of XDEM to the calcination process of a $CaCO_3$ sample in the powder state. The proposed numerical model accounts for gas flow via an open source CFD code, heat and mass transfer with particles and a 1D conductive–diffusive model for heat and mass transport inside each single particle. Predictions are validated with the experimental data documented by Gieorgieva et al. [5], where conduction with the solid walls plays a major role in the process.

This model should represent a first step towards the development of a soft sensor for the prediction of thermal and chemical variables inside a cement kiln. To that end, a complex CFD–DEM model will estimate the accuracy of simplified 1D models, which are suited for online implementations (rapid calculation times, etc.).

2. Extended Discrete Element Method (XDEM)

The Extended Discrete Element Method (XDEM) is an advanced multi-physics and numerical simulation framework in which the dynamics of granular material or particles described by the classical discrete element method (DEM) (Cundall [22] and Allen [23]) are extended by additional properties such as the thermodynamic state, and the stress/strain for each particle (Peters [14] and Mahmoudi [15]). In addition, the XDEM concept covers the coupling between discrete and continuous phases simultaneously. Thus, within this framework, continuous numerical approaches such as CFD (Computational Fluid Dynamics) and/or Finite Element Analysis (FEA) are coupled to discrete approaches in order to address numerous challenges in engineering e.g. drug production, agriculture and food processing industries, mining, construction and agricultural machinery, metal manufacturing, energy production and systems biology. Hence XDEM is considered as a Euler–Lagrange model, where the fluid phase is continuous, but each solid particle is tracked with a Lagrangian approach.

For a better understanding of the symbols used in the following subsections the reader is invited to review Section 5 of this paper.

2.1. Modeling fluid flow in porous media

The gas phase is solved according to a CFD model for porous media. One important quantity which characterizes a porous medium is its porosity ϵ_f. Porosity can be computed as the ratio between the void space and total volume of the packed bed, ranging between 0 and 1:

$$\epsilon_f = \frac{V_{void}}{V_{total}}. \tag{2}$$

The fluid model is based on a description of the flow as a continuous flow with averaging of the relevant variables on a coarser level, with respect to the sizes of the individual channels of the tortuous void space. This is done through the introduction of a Representative Elementary Volume (REV), which respects the following condition:

$$L_g << L_{REV} << L \tag{3}$$

with L being the characteristic length of the problem, L_{REV} the linear dimension of the REV, and L_g the microscopic length scale, i.e. the one associated with void dimension.

State variables, velocity and chemical concentrations inside the gas phase are averaged over the REV ($\langle\rangle$ symbol in the following equations).

The equations constituting the model are deduced from those used for a laminar flow (this assumption is justified by the conditions of the present setup, with a Reynolds Number ranging between 5.032 and 5.832 [5]).

2.1.1. Continuity equation

The continuity equation has the following expression:

$$\frac{\partial}{\partial t}\left(\epsilon_f\left\langle\rho_f\right\rangle^f\right)+\vec{\nabla}\cdot\left(\epsilon_f\left\langle\rho_f\right\rangle^f\left\langle\vec{v}_f\right\rangle^f\right)=\dot{m}_{s,f}^{'''} \tag{4}$$

where $\dot{m}_{s,f}^{'''}$ is a source term that accounts for mass transfer from the solid to the gas phase and vice versa. This "mass source" term is obtained from the mass fluxes between particles and fluid as will be explained in Section 2.3.

2.1.2. Momentum equation

The conservation equation of linear momentum is written:

$$\begin{aligned}&\frac{\partial}{\partial t}\left(\epsilon_f\left\langle\rho_f\right\rangle^k\left\langle\vec{v}_f\right\rangle^f\right)+\vec{\nabla}\cdot\left(\epsilon_f\left\langle\rho_f\right\rangle^f\left\langle\vec{v}_f\vec{v}_f\right\rangle^f\right)\\&=\vec{\nabla}\cdot\left(\epsilon_f\left\langle\vec{\tau}_f\right\rangle^f\right)-\frac{\mu_f}{K}\epsilon_f^2\left\langle\vec{v}_f\right\rangle^f-C\left\langle\rho_f\right\rangle^f\epsilon_f^3\left|\left\langle\vec{v}_f\right\rangle^f\right|\left\langle\vec{v}_f\right\rangle^f.\end{aligned} \tag{5}$$

K and C are calculated according to the characteristics of the packed bed, as follows:

$$K=\frac{D_p^2\epsilon_f^3}{150\left(1-\epsilon_f\right)^2} \tag{6}$$

$$C=\frac{1.75\left(1-\epsilon_f\right)}{D_p\epsilon_f^3}. \tag{7}$$

2.1.3. Energy equation

The conservation equation of energy is written:

$$\begin{aligned}&\frac{\partial}{\partial t}\left(\epsilon_f\left\langle\rho_f\right\rangle^f\left\langle h_f\right\rangle^f\right)+\left(\epsilon_f\left\langle\rho_f\right\rangle^f\left\langle\vec{v}_f h_f\right\rangle^f\right)\\&=-\nabla\cdot\left\langle\vec{q}^{''}\right\rangle+\frac{\partial p_f}{\partial t}+\left\langle\vec{v}_f\right\rangle\cdot\nabla\left\langle p_f\right\rangle+\left\langle Q_{V,f}\right\rangle+q_{s,f}^{'''}\end{aligned} \tag{8}$$

where $\langle Q_{V,f}\rangle$ accounts for the energy released due to reactions within the gas phase whereas $q_{s,f}^{'''}$ accounts for the heat exchange between the solid and the gas phases as explained in Section 2.3.

2.1.4. Species equation

The conservation equation for species i in the continuum is:

$$\frac{\partial}{\partial t}\left(\epsilon_f\left\langle\rho_{f,i}\right\rangle^f\right)+\vec{\nabla}\cdot\left(\epsilon_f\left\langle\rho_{f,i}\right\rangle^f\cdot\left\langle\vec{V}_f\right\rangle^f\right)=\sum_{i=1}^{N}\dot{m}_{s,f,i}^{'''} \tag{9}$$

where $\dot{m}_{s,f,i}^{'''}$ is the volumetric source accounting for the mass transferred from/to the particulate (Section 2.3).

2.2. Discrete modeling

The discrete modeling of the powder material is based on the Discrete Particle Method (DPM). DPM is a numerical tool, which deals with both the dynamics and the chemical conversion of particulate material using a Lagrangian approach for each particle. However, predictions of solely motion or conversion in a decoupled mode are also applicable.

In DPM conversion, a discrete particle is considered to consist of different multicomponent phases: solid, inert (i.e. solid phase which does not undergo chemical reactions), liquid, and gases, with gaseous phases occupying porous volumes inside each particle. DPM is based on the assumption of thermal equilibrium inside each particle; this means the temperature distribution of each phase is the same as the others. This assumption is based on the assessment of the ratio of heat transfer by conduction to the rate of heat transfer by convection expressed by the Peclet number, as described by Peters [24] and Kansa et al. [25]. Relevant thermochemical processes are described by a set of one-dimensional and transient differential conservation equations for mass, species, momentum and energy, as well as the state equation.

2.2.1. Conservation of mass for gas phase

The conservation of mass for gas within the pore volume of a porous particle is written as follows:

$$\frac{\partial}{\partial t}\left(\epsilon_p\left\langle\rho_f\right\rangle^f\right)+\vec{\nabla}\cdot\left(\epsilon_p\left\langle\rho_f\right\rangle^f\left\langle\vec{v}_f\right\rangle^f\right)=\dot{m}^{'''}{}_{s,p} \tag{10}$$

where the term on the right hand side accounts for mass transfer between the fluid within the pore of the particle or the solid phase with gas as a result of water evaporation or chemical reactions. ϵ_p denotes particle porosity, ρ_f gas phase density and $\vec{v}_f$ advective velocity. The gas density (ρ_f) is given by the sum of partial densities of species present in the gas phase as:

$$\rho_f=\sum_{i=1}\rho_i. \tag{11}$$

2.2.2. Conservation of species in gas phase

For conservation of individual gaseous species within the void space of a porous particle the following equation is applied:

$$\frac{\partial\left(\epsilon_p\left\langle\rho_{i,g}\right\rangle^g\right)}{\partial t}+\frac{1}{r^n}\frac{\partial}{\partial r}\left(r^n\left\langle\rho_{i,g}\right\rangle^g\left\langle u_g\right\rangle\right)=\frac{1}{r^n}\frac{\partial}{\partial r}\left(r^n D_i\epsilon_p\frac{\partial}{\partial r}\left\langle\rho_{i,g}\right\rangle^g\right)+\epsilon_p\sum_k\dot{\omega}_{k,i,g} \tag{12}$$

where $\langle\rho_{i,g}\rangle$ denotes the intrinsic partial density of gaseous species i, D_i the molecular diffusion coefficient, $\langle u_g\rangle$ the extrinsic velocity and $\dot{\omega}_{k,i}$ sources or sinks of species i resulting from reaction k.

2.2.3. Conservation of mass for liquid and solid phases

The conservation of mass for liquid and solid species is based on the conversion rates $\dot{\omega}_k$ by chemical reactions:

$$\frac{\partial\rho_{i,liquid}}{\partial t}=\sum_k M_i\cdot\dot{\omega}_{k,i,liquid} \tag{13}$$

$$\frac{\partial\rho_{i,solid}}{\partial t}=\sum_k M_i\cdot\dot{\omega}_{k,i,solid}. \tag{14}$$

Consequently, the porosity of a single particle ϵ_p is evaluated according to the conservation of species and conservation of mass for the different phases.

In this paper, $CaCO_3$ calcination is modeled as an irreversible finite rate reaction involving one reactant (Eq. (1)), with reaction rate $\dot{\omega}$:

$$\dot{\omega}=k(T)\cdot[CaCO_3] \tag{15}$$

where the rate constant, $k(T)$, depends on the temperature change and it is calculated following the Arrhenius law:

$$k(T)=k_0\cdot e^{\frac{-E_a}{RT}}. \tag{16}$$

2.2.4. Conservation of linear momentum

Transport of gaseous species within the pore space of the particle is considered to obey Darcy's law. Thus, momentum conservation states:

$$-\frac{\partial\left(\epsilon_f p\right)}{\partial x}=\frac{\mu_f\epsilon_f}{K}\left\langle v_f\right\rangle \tag{17}$$

where K is the so-called permeability characterizing the morphology of the porous particle, μ_g is the viscosity of the fluid, p is the pressure and $\langle u_g\rangle$ the average of the advective velocity.

2.2.5. Conservation of energy

The energy equation is based on the homogeneous model for a porous medium as described by Faghri [26] and written as:

$$\frac{\partial\left\langle\rho c_p T\right\rangle}{\partial t}=\frac{1}{r^n}\frac{\partial}{\partial r}\left(r^n\lambda_{eff}\frac{\partial\langle T\rangle}{\partial r}\right)+\sum_{k=1}^{l}\dot{\omega}_k H_k \tag{18}$$

where λ_{eff} is the effective thermal conductivity and its calculation is described in [24]. The source term on the right hand side represents the release or consumption of energy due to chemical reactions, H_k is the enthalpy of reaction k.

The previous formulation (Eqs. 12, 18) allows the geometry of the particle to be one of the following: infinite plate $n=0$, infinite cylinder $n=1$ or a sphere $n=2$.

2.2.6. Equation of state

Assuming thermodynamic equilibrium within the intra-particle fluid, and considering it as a perfect gas, the equations of state in terms of the two state variables, temperature T and gas density ρ, are:

$$p=\rho R_v T \tag{19}$$

$$h=c_p T. \tag{20}$$

To complete the mathematical model, boundary conditions must be provided. A symmetric boundary condition is applied for the center of a spherical particle:

$$-\lambda_{eff}\frac{\partial\langle T\rangle}{\partial r}\bigg|_{r=0}=0 \tag{21}$$

$$-D_i\frac{\partial\left\langle\rho_{i,g}\right\rangle^g}{\partial r}\bigg|_{r=0}=0. \tag{22}$$

The following boundary conditions for heat transfer and mass transfer of gaseous species are applied at the surface of the particle:

$$-\lambda_{eff}\frac{\partial\langle T\rangle}{\partial r}\bigg|_{r=R}=\alpha\left(T_R-T_\infty\right)+\dot{q}''_{p,cond}+\dot{q}''_{p,rad} \tag{23}$$

$$-D_i\frac{\partial\left\langle\rho_{i,g}\right\rangle^g}{\partial r}\bigg|_{r=R}=\beta_i\left(\left\langle\rho_{i,g}\right\rangle^g-\rho_{i,\infty}\right)+\dot{m}''_{i,g} \tag{24}$$

where T_∞, and $\rho_{i,\infty}$ denote ambient gas temperature and gas partial density of species i in the ambient, respectively. T_R and $\rho_{i,g}$ are the particle temperature and the partial density of species i at the particle surface, respectively. The heat fluxes on the right hand side account for radiative heat exchange with the surroundings or conductive heat transport through physical contact with neighboring particles or walls. Walls may be described by particles or a set of particles with thermal interaction. The term $\dot{m}''_{i,g}$ accounts for the exchange of species with the ambient gas by advective transport through the surface. A full description of the model is reported in [24] and [27]. α and β are heat transfer coefficient and mass transfer coefficient, respectively.

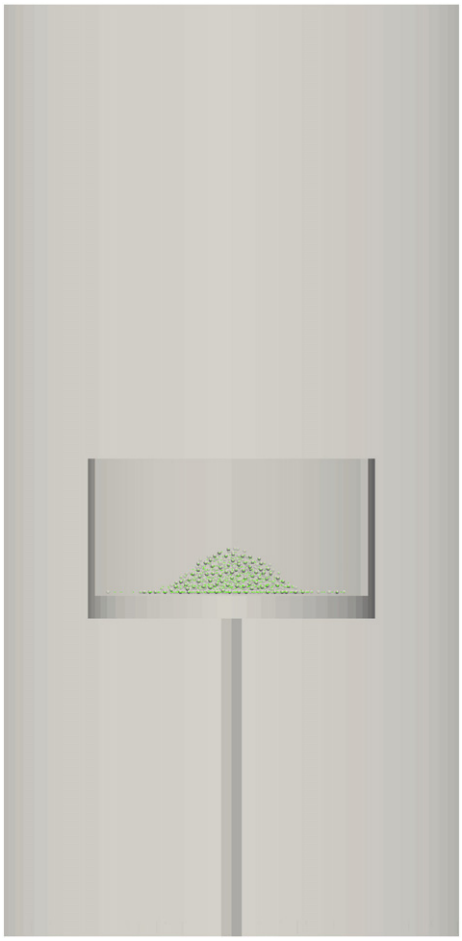

Fig. 1. Geometry of the numerical model.

2.3. Discrete-continuous coupling

Heat exchange between the solid and fluid phases is governed by the thermal conditions at the interface. Considering all the N particles in a REV leads to the following formulation for the volumetric source/sink term in the energy equation:

$$\dot{\vec{q}}'''_{s,f}=\sum_{j=1}^{N}\left\langle\frac{A_{p,j}}{V_{REV}}\alpha_j\left(T_{p,j}-T_f\right)\right\rangle. \tag{25}$$

Table 1
Experimental setup [5].

Fluid properties:		
Volumetric flow	25	$\frac{cm^3}{min}$
Composition		
N_2	99.9999	%
Solid phase properties:		
Total mass	5	mg
Composition		
$CaCO_3$	100	%
Kinetic parameters:		
Pre-exponential factor (k)	7.41e16	min^{-1}
Activation energy (E_a)	325.1	$\frac{kJ}{mol}$
Crucible size:		
Height	3	mm
Diameter	6	mm

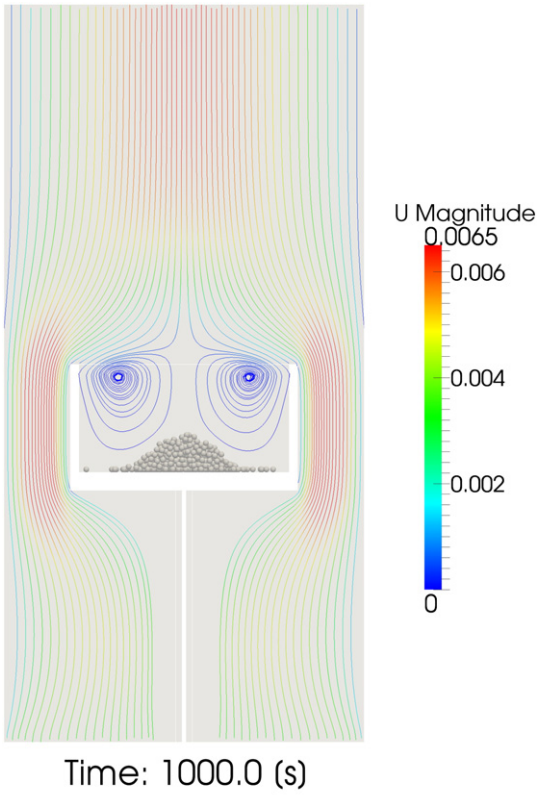

Fig. 2. Streamlines in the gas field.

The amount of mass exchange of species *i* between a particle and the gas phase $\left(\dot{m}''_{p,f,i}\right)$ is related to the local conditions at the interface as well as to β (mass transfer coefficient):

$$A_p\beta_i\left(\left\langle rho_{p,i,g}\right\rangle^{g}-\rho_{f,i}\right)+A_p\cdot\dot{m}''_{p,i,g}=\dot{m}'''_{p,f,i}V_{REV} \tag{26}$$

with $\dot{m}''_{p,i,g}$ being the advective contribution. For a given quantity of N particles in a REV the mass source term becomes:

$$\dot{m}'''_{s,f,i}=\sum_{j=1}^{N}\left(\dot{m}'''_{p,f,i}\right)_j. \tag{27}$$

In order to obtain the value of the overall fluid mass volumetric source term, a summation of all the species mass source/sink terms *M* is performed as follows:

$$\dot{m}'''_{s,f}=\sum_{i=1}^{M}\sum_{j=1}^{N}\left(\dot{m}'''_{s,f,i}\right)j. \tag{28}$$

A correct evaluation of α and β coefficients is fundamental to properly establish the magnitudes of heat and mass transfers. XDEM calculates these two quantities according to Nusselt, Reynolds and Sherwood numbers of the fluid field:

$$\alpha=Nu\frac{\lambda_f}{D_p} \tag{29}$$

$$\beta_i=Sh\frac{D_{ij}}{D_p}. \tag{30}$$

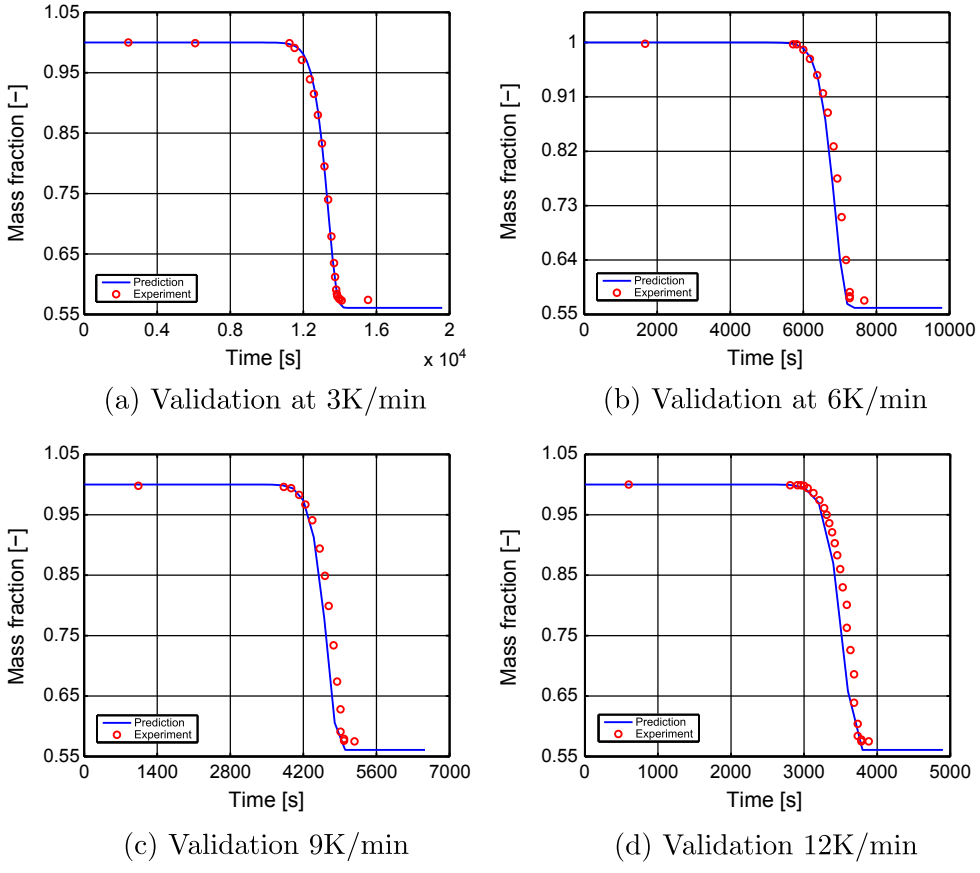

Fig. 3. Comparison of numerical predictions with experimental data.

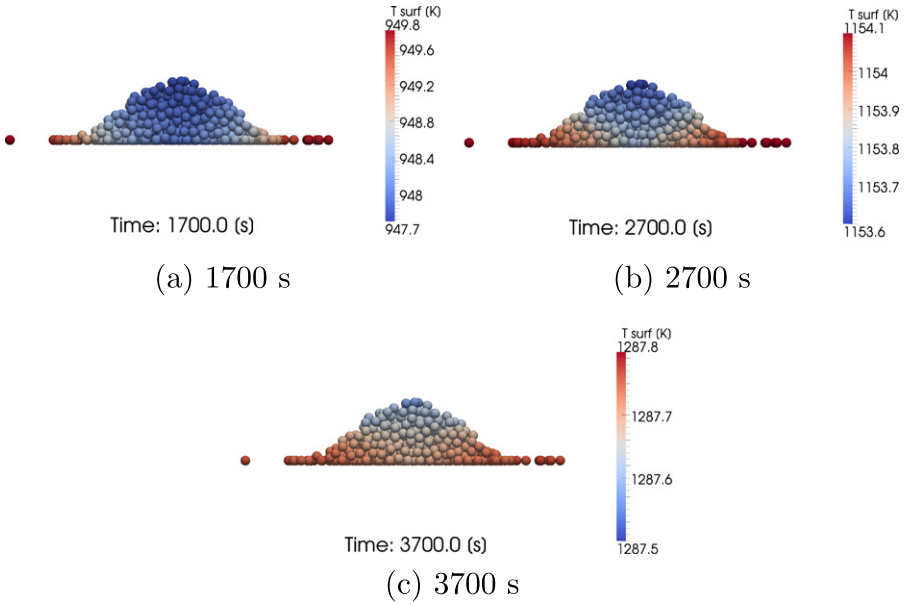

Fig. 4. Predictions of particulate surface temperature during $CaCO_3$ decomposition at 12K/min.

The Nusselt number (Nu) is calculated according to the suitable porous media, semi-empirical correlations reported in [13] and [27].

3. Predicted results

In this section, the results are presented for the XDEM numerical prediction of the $CaCO_3$ decarbonation process, performed in non-isothermal conditions.

The setup is the one used by Gieorgieva [5] in his experimental tests. In [5] small samples of $CaCO_3$ of about 5 ± 0.1 mg were loaded without pressing into an open 6 mm diameter and 3 mm high platinum crucible. Thermogravimetrical measurements were carried out in a flow of nitrogen (99.999 %) at a rate of 25cm^3/min under non-isothermal conditions. The gas flow came from the bottom of a 10 mm diameter and 20 mm long pipe; the crucible was placed in the middle of the pipe. An electrical furnace provided controlled heating of the samples up to 1000 °C, at 4 different rates: 3, 6, 9, 12 K/min.

The present model provides a full description of the previous experimental setup. Positions of the particles were obtained by running the dynamic module of the DPM as described by Michael [28]. Thus, particles were deposited by gravity at the bottom of the crucible. The experimental setup was chosen for validation of the $CaCO_3$ calcining model as it offers the possibility to assess the prediction of chemical reactions and heat and mass transfer in non-isothermal conditions. This is very important in order to ascertain the applicability of XDEM in future studies concerning the prediction of thermal and chemical phenomena inside rotary cement kilns.

The geometry of the numerical model is shown in Fig. 1. The crucible is placed inside the reaction chamber. A nitrogen gas flow comes from the bottom of the furnace and surrounds the crucible. The walls of the furnace and the gas at the inlet are assumed to be at temperatures which exactly follow the heating rate. The heat flows by radiation from the walls of the furnace to the crucible and by convection from the gas to the crucible. The particles are heated by the crucible via conduction and radiation. The parameters of the numerical model are summarized in Table 1.

Fig. 2 shows streamlines for the gas velocity field. As can be noted, recirculating vortices inside the crucible provide a further heat exchange by convection between the gas and the particles; they also allow CO_2 removal from the sample.

Validation of the numerical model was performed by comparison between the experimental TG curves and predictions for mass loss. The kinetic parameters used in the numerical prediction are the same as obtained by Gieorgieva [5]: the pre-exponential factor is 7.41e16 min^{-1}, activation energy is 325.1kJ/mol. Experimental and numerical TG curves are reported in Fig. 3a, b, c, d. A good agreement was found between the experimental and the numerical data. The experimental and numerical TG curves show the same trend when changing the heating rate. In both cases the curves tend to shift to the right as the heating rate increases.

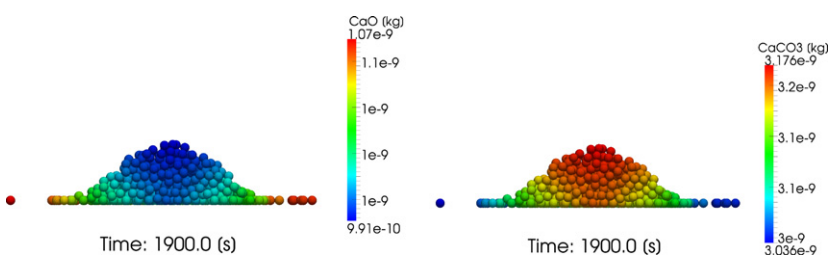

Fig. 5. Solid species mass.

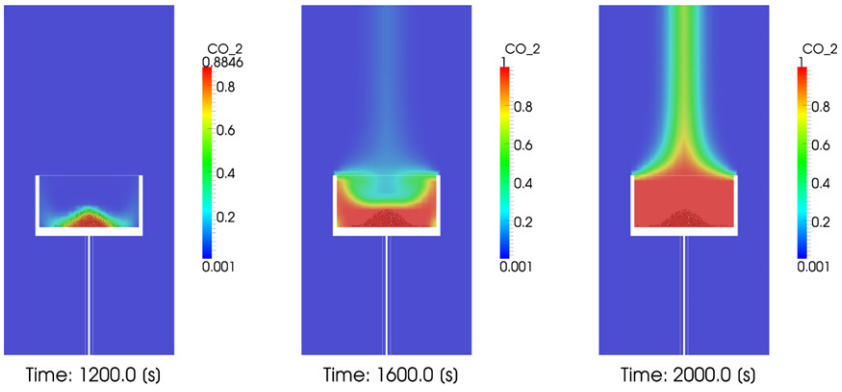

Fig. 6. CO_2 concentration in the gas phase.

Fig. 4a, b, c shows the surface temperature of particles of the sample on a vertical cross-section at 3 different times. Consistent with the experimental setup description, heating proceeds from the bottom to the top of the sample. This means that the conductive and radiative heating provided by the walls of the crucible is preponderant with respect to the convective contribution of the gas.

As a consequence of the temperature distribution inside the sample, the reaction starts earlier for particles at the bottom. Fig. 5a, b shows CaO and $CaCO_3$ mass fractions for each particle on the same cross-section, at the moment when decarbonation takes place.

Fig. 6a, b, c shows CO_2 concentration in the gas phase, at 3 different time steps. As can be noted, CO_2 is produced inside the particles and flows outside, in the gas field. While the reaction is proceeding, CO_2 is forced out of the crucible by the gas flowing from the bottom.

Fig. 7 shows the evolution of porosity during heating, for two particles of the sample. As a consequence of solid phase consumption due to the dissociation of CO_2, porosity increases with a rate that is proportional to the speed of reaction.

The results show the capability of XDEM to correctly predict chemical reactions conducted in non-isothermal conditions, involving solid reactants. The model represents a first step towards understanding all the thermal and chemical phenomena occurring inside rotary cement kilns where several reactions and particulate dynamics are taking place. Moreover, this contribution also shows that XDEM can be seen as a general approach for accurately estimating the complex process of cement production.

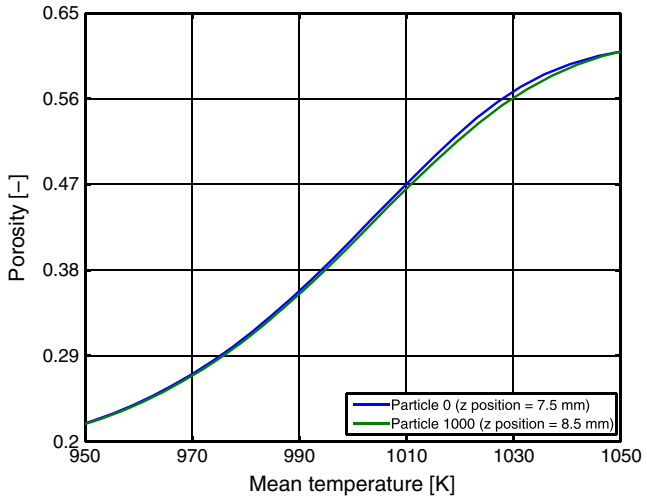

Fig. 7. Evolution of porosity for two different particles.

4. Conclusions

The XDEM approach was successfully applied to the prediction of the calcination process in non-steady thermal conditions, involving a small sample of calcium carbonate in the powder state. The good agreement with experimental data demonstrated the capability of the XDEM approach to account for the thermal exchange between the gas phase and the powder phase, the chemical conversion of the solid phase of each particle, CO_2 production and diffusion from particles to the gas phase, radiative and conductive heat transfer inside the packed bed and also heat transfer between the packed bed and the external walls.

This model represents a first step towards the development of a detailed CFD–DEM description of all the thermochemical phenomena taking place inside a cement kiln system. The final CFD–DEM model will be implemented in order to provide an estimation of accuracy for a soft sensor based on a simplified thermochemical 1D model, which is suitable for online implementation (rapid calculation times, etc.).

Nomenclature

Subscripts

f	fluid
g	gas
k	phase
p	particle
∞	ambient

Greek symbols, units

α	heat transfer coefficient, W/m^2K
β	mass transfer coefficient, m/s
ϵ	porosity, —
λ	heat conductivity, W/mK
μ	dynamic viscosity, kg/ms
ξ	mass fraction, —
ρ	density, kg/m^3
$\dot{\omega}$	reaction source, mol/m^3s

Latin symbols, units

A	area, m^2
c_p	specific heat capacity at constant pressure, J/kgK
d	diameter, m
D	diffusion coefficient, m^2/s
h	Enthalpy, $\frac{J}{kg}$
K	permeability, m^2
m	mass
$\dot{m}$	mass flow rate, kg/s
$\dot{m}'''$	mass source, kg/m^3s

M	molar mass, kg/mol
p	pressure, Pa
$\dot{q}''$	heat flux, W/m^2
r	radius; radial coordinate, m
R	radius, m
$\mathcal{R}$	universal gas constant, J/molK
R_v	specific gas constant, J/kgK
S	surface, m^2
t	time, s
T	temperature, K
v	velocity, m/s
V	volume, m^3

References

[1] [link]. URL www.globalcement.com/news/item/1939-pca-forecasts-us -cement-consumption-to-grow-by-97-from-2014.
[2] A Neuro-Fuzzy Controller for Rotary Cement Kilns.
[3] M. Schneider, M. Romer, M. Tschudin, H. Bolio, Sustainable cement production — present and future, Cem. Concr. 41 (2011) 642–650.
[4] P. Kadlex, B. Gabrys, S. Strandt, Data-driven soft sensors in the process industry, Comput. Chem. Eng. 33 (2009) 795–814.
[5] V. Gieorgieva, L. Vlaev, K. Gyurova, Non-isothermal degradation kinetics of caco3 from different origin, Journal of Chemistry.
[6] H. Mikulcic, E. von Berg, M. Vujanovic, Numerical modelling of calcination reaction mechanism for cement production, Chem. Eng. Sci. 69 (2012) 607–615.
[7] R.H. Borgwart, Calcination kinetics and surface area of dispersed limestone particles, AICHE J. 31 (1985) 103–111.
[8] A. Bes, Dynamic process simulation of limestone calcination in normal shaft kilns, Ph.D. Thesis.
[9] M. Mohr, Numerische simulation der simultanen reaktion von kalkstein und kohle bei der zementherstellung, Ph.D. Thesis.
[10] M. Slack, R. Prasad, A. Bakker, F. Boysan, Advances in cyclone modelling using unstructured grids, TranslChemE 78 (2000) 1098–1104.
[11] Z. Hu, J. Lu, L. Wang, Numerical simulation study on gas–solid two phase flow in pre-calciner, Commun. Nonlinear Sci. Numer. Simul. 11 (2006) 440–451.
[12] A. A. Estupinan Donoso, B. Peters, {XDEM} employed to predict reduction of tungsten oxide in a dry hydrogen atmosphere, International Journal of Refractory Metals and Hard Materials.
[13] A. Estupinan Donoso, F. Hoffmann, B. Peters, Extended discrete element method used for convective heat transfer predictions, Int. Rev. Mech. Eng. 7 (2) (2013) 328–336.
[14] B. Peters, X. Besseron, A. Estupinan, F. Hoffmann, M. Michael, M. A., The extended discrete element method (XDEM) applied to drying of a packed bed, IFRF Journal.
[15] A.H. Mahmoudi, F. Hoffmann, B. Peters, Application of XDEM as a novel approach to predict drying of a packed bed, Int. J. Therm. Sci. 75 (2014) 65–75.
[16] B. Peters, Validation of a numerical approach to model pyrolysis of biomass and assessment of kinetic data, Fuel 90 (6) (2011) 2301–2314.
[17] B. Peters, Prediction of pyrolysis of pistachio shells based on its components hemicellulose, cellulose and lignin, Fuel Process. Technol. 92 (2011) 1993–1998.
[18] B. Peters, Applying a detailed reaction mechanism to pyrolysis of *Miscanthus giganteus*, J. Appl. Anal. Pyrol. 91 (2011) 352–358.
[19] F. Hoffmann, B. Peters, An integrated approach to model blast furnaces, Proceedings of METEC InSteelCon 2011, 4th International Conference on Modelling and Simulation of Metallurgical Processes in Steelmaking (STEELSIM), 2011.
[20] F. Hoffmann, B. Peters, Extended discrete element method (XDEM) to model heterogeneous reactions in packed beds, Proceedings of PARTEC 2013 — International Congress on Particle Technology, 2013.
[21] T. Bluhm-Drenhaus, E. Simsek, S. Wirtz, V. Scherer, A coupled flui dynamic-discrete element simulation of heat and mass transfer in a lime shaft kiln, Chem. Eng. Sci. 65 (2010) 2821–2834.
[22] P.A. Cundall, O.D.L. Strack, A discrete numerical method for granular assemblies, Geotechnique 29 (1979) 47–65.
[23] M. P. Allen, D. J. Tildesley, Computer simulation of liquids, Claredon Press Oxford.
[24] B. Peters, Thermal conversion of solid fuels, WIT press.
[25] E.J. Kansa, H.E. Perlee, R.F. Chaiken, Mathematical model of wood pyrolysis including internal forced convection, Combust. Flame 29 (1977) 311–324.
[26] A. Faghri, Y. Zhang, Transport Phenomena in Multiphase Systems, Elsevier, 2006.
[27] F. Hoffmann, Modelling heteregeneous reactions in packed beds and its application to the upper shaft of a blast furnace, Ph.D. Thesis.
[28] M. Michael, A discrete approach to describe the kinematics between snow and a tire tread, Ph.D. thesis, University of Luxembourg (2014).